Multiresolution-based adaptive schemes for Hyperbolic Conservation Laws

Guillaume Chiavassa[1], Rosa Donat[2], and Siegfried Müller[3]

[1] LATP and ESM2, Technopôle de Château-Gombert, 13451 Marseille Cedex 20, France guillaume.chiavassa@esm2.imt-mrs.fr
[2] Departamento de Matematica Aplicada, Universidad de Valencia, 46100 Burjassot (Valencia), Spain donat@uv.es
[3] Institut für Geometrie und Praktische Mathematik, RWTH Aachen, 52056 Aachen, Germany mueller@igpm.rwth-aachen.de

Summary. Starting in the early nineties, wavelet and wavelet-like techniques have been successfully used to design adaptive schemes for the numerical solution of certain types of PDE. In this paper we review two representative examples of the development of such techniques for Hyperbolic Conservation Laws.

1 Introduction

In the context of Hyperbolic Conservation Laws (HCL henceforth), singularities and sharp transition regions model such important physical phenomena as the formation and evolution of shock waves. There is a general agreement that shock related phenomena need an adequate numerical treatment that usually involves a considerable increase in computational resources.

Solutions to systems of HCLs tend to be highly nonuniform in their spatial behavior. Large regions of smooth, slowly varying behavior are separated by highly localized transition regions of non-smooth behavior. Fine grids are often necessary in order to resolve adequately regions of strong variation, but uniformity in the computational meshes necessarily implies that the solution is over-resolved in smoothness regions, usually the largest part of the computational domain.

The need to solve realistic problems has motivated the development of adaptive techniques, for which the computational effort concentrates near regions where singularities or sharp transitions occur.

Classical Adaptive Mesh Refinement (AMR) techniques [BO84, BC89] rely on a sequence of nested grids of increasing resolution and on certain error estimators that seek to determine locally whether the current resolution of the numerical solution is sufficient or a finer grid is necessary. These techniques involve a considerable effort in programming and data management but are now routinely used in realistic simulations.

In recent years, the development of the theory of wavelets has provided an additional tool to design numerical schemes that seek to adapt the computational resources to the local structure of the solution to be computed.

Working within a Galerkin framework, Liandrat and Tchamitchian [LT] developed a numerical scheme in which adaptive refinement is implemented by adding layers of successive "details" that locally increase the resolution of the approximation. Time adaptivity was incorporated in [BMP92], where the authors present a wavelet-based numerical method for hyperbolic and parabolic PDEs that adapts the space and time resolutions to the properties of the PDE and the local structure of the solution.

Being translates and dilates of a single function, wavelet bases are often too 'rigid' for certain applications. Indeed, in [LT, BMP92] only periodic problems for scalar hyperbolic and parabolic equations in one dimension are handled, mainly because of various technical difficulties related to the wavelet basis considered. Even though some of the problems related to the poor representation of boundaries by wavelet basis have been addressed in recent years (see [Coh03, Dah97] for good reviews on wavelet methods for PDEs), successful multiresolution-based adaptive techniques for HCL have followed instead the path laid out by A. Harten in his seminal work [Har95].

In the early 90's, A. Harten developed a general framework for multiresolution (MR) that exhibits a larger degree of flexibility, while retaining many of the properties associated to wavelet-decompositions. A distinctive feature of Harten's framework is that a discrete data set is always interpreted as the result of the application of a particular discretization operator on a function belonging to an appropriate functional space. This feature is well suited for computing solutions to PDEs by numerical techniques, since the values obtained are interpreted as discrete realizations of the solution on a computational mesh.

A MR decomposition of a discrete realization of a given function gives precise information on the local regularity of that function. Harten's adaptive strategy is based on the smoothness information contained on an appropriate MR decomposition of the numerical data obtained, at each time step, by an underlying numerical scheme.

In its simplest implementation the goal of the MR-based adaptive scheme is, essentially, to gain computational time while remaining within the same accuracy as the *reference* scheme, i.e. the scheme on the finest computational mesh for which the user is pleased with the computational results. Successful implementations of this strategy have been carried out for two-dimensional Cartesian meshes [BH95, BH97, CD01], curvilinear meshes [DGM00] and unstructured meshes [Abg97, CDKP00, BOLR01].

A more elaborate implementation has been developed in [CKMP03]. Here, the MR decomposition of the numerical data is used to reduce not only the computational cost, but also the memory requirements of the computation, while remaining within the same accuracy as the *reference* scheme. The implementation in [CKMP03] is indeed a spatial AMR technique, in which adaptive

refinements are based on the smoothness information obtained from the MR decomposition of the data.

In this paper we shall review these two main directions in which Harten's methodology for the design of adaptive schemes for HCLs has evolved during the last ten years. The paper is organized as follows: In section 2 we briefly describe the essential ingredients of Harten's framework for MR, with particular attention to the interpolatory and cell-average frameworks. Section 3 describes the basic strategy of MR-based adaptive schemes. In section 3.1 we briefly review the cost-reduction implementation and in section 3.2 the fully adaptive one. We close in section 4 with a summary.

2 Data Representation and Multiscale Analysis

The numerical values obtained by a given numerical scheme are understood as approximations to a discrete realization of the solution on an underlying computational mesh. When using a sufficiently robust scheme, these numerical values reflect in one way or another the behavior of the true solution. In those regions where the solution is smooth, the discrete data displays a 'smooth discrete behavior'. At shocks and/or contact discontinuities, the discontinuous behavior of the true solution is represented by a sharp profile. In fact, the robustness of the scheme is often measured by the ability to represent a shock transition as a sharp, oscillation-free, discrete profile.

Smoothness regions can be handled with rather unsophisticated (and non-expensive) numerical techniques, while compression regions and shocks require a very specialized numerical treatment. A multiscale decomposition of the numerical solution at each time step can provide the necessary information about the local smoothness of the underlying data to allow for an adaptive computation.

A multiresolution (MR) decomposition of a discrete data set is an alternative (i.e. equivalent) representation that encodes the information as a coarse realization of the given data set plus a sequence of detail coefficients of ascending resolution. The detail (scale, wavelet) coefficients represent the *difference in information* between consecutive resolution levels.

In the following we give a brief overview of the core ingredients of Harten's MR concept namely: (i) a sequence of nested discretization operators and (ii) a sequence of *consistent* reconstruction operators.

Discretization and Decimation The starting point is a sequence of vector spaces V_l, $l \in \mathbb{N}_0$. The index l represents the resolution level (increasing l means more resolution). For the application that we have in mind, the resolution levels are specified by a sequence of computational meshes $\mathcal{G}_l = \{\Omega_{l,k}\}_{k \in J_l}$, $l = 0, \ldots, L$ on a domain Ω, and V_l represents a linear space of discrete data, related to $\mathcal{G}_l$ via a particular *discretization operator*.

The discretization operators are linear operators acting on a function space $\mathcal{D}_l : \mathcal{F} \to V_l$ ($\mathcal{F}$ is usually the solution space for the PDE). Given $u \in \mathcal{F}$, $\mathcal{D}_l u$

assigns a discrete value to each $\Omega_{l,k} \in \mathcal{G}_l$,

$$\bar{u}_k^l = (\mathcal{D}_l u)_k =: \mathcal{A}(\Omega_{l,k})u \qquad \forall \Omega_{l,k} \subset \mathcal{G}_l. \tag{1}$$

The grid *elements*, $\Omega_{l,k}$ can be either grid-points or mesh-cells (structured or unstructured). The chosen notation reflects the fact that we think of the discretization as an *averaging operator*. For point-value discretizations, the *elements* of the grid are its nodes and the averaging is done with respect to Dirac's delta function. For cell-average discretizations, the *elements* of the mesh are the cells (quadrilateral, triangles, hexahedra) and the averaging is done with respect to the indicator function of each cell.

To obtain multiscale decompositions associated to a sequence of meshes $\{\mathcal{G}_l\}$ on a domain $\Omega \subset \mathbb{R}^d$, the associated discretization operators $\mathcal{D}_l$ have to satisfy two essential properties

1. $\mathcal{D}_l$ is onto.
2. The null spaces satisfy $\mathcal{N}(\mathcal{D}_l) \subset \mathcal{N}(\mathcal{D}_{l+1})$.

Property 2 gives the sequence $\{\mathcal{D}_l\}$ a *nested* structure. For our intended application, this property derives from the structure of the averaging operator and a nested structure in the sequence $\{\mathcal{G}_l\}$, i.e. each cell $\Omega_{l,k}$ on level l can be subdivided into subcells $\Omega_{l+1,r}$ on the finer level $l+1$ so that

$$\Omega_{l,k} = \cup_{r \in \mathcal{M}_{l,k}} \Omega_{l+1,r}. \tag{2}$$

As a consequence of properties 1 and 2 we can associate to the sequence $\{\mathcal{D}_l\}$ a sequence of *decimation operators*, by which coarse data is obtained from fine data [Har96]: If $u \in \mathcal{F}$ and $\bar{u}^m = \mathcal{D}_m u$ for each m, then $\bar{u}^l = D_{l+1}^l \bar{u}^{l+1}$ for all l. For local averaging operators we obtain

$$D_{l+1}^l : V_{l+1} \longrightarrow V_l \qquad (D_{l+1}^l \bar{u}^{l+1})_k = \sum_{r \in \mathcal{M}_{l,k}} m_{k,r}^{l,0} \bar{u}_r^{l+1}, \quad k \in J_l \tag{3}$$

where the coefficients $m_{k,r}^{l,0}$ depend *only* on the sequence $\{\mathcal{D}_l\}$.

Reconstruction and Prediction To represent the difference between discrete values on two consecutive resolution levels, a sequence of *consistent* reconstruction operators is introduced. For each resolution level $\mathcal{R}_l : V_l \to \mathcal{F}$, where consistency means that

$$\mathcal{D}_l \mathcal{R}_l \bar{u}^l = \bar{u}^l \qquad \forall \bar{u}^l \in V_l. \tag{4}$$

Notice that if $\bar{u}^l = \mathcal{D}_l u$, $u \in \mathcal{F}$, then $\mathcal{R}_l \bar{u}^l$ is interpreted as an approximation to u. In general $u \neq \mathcal{R}_l \bar{u}^l$, but (4) implies that u and $R_l \bar{u}^l$ have the same discrete information on $\mathcal{G}_l$.

In our context, $\mathcal{R}_l \bar{u}^l$ is constructed by defining appropriate piecewise polynomial functions. For each element $\Omega_{l,k} \in \mathcal{G}_l$ we construct a polynomial $R_{l,k}^N : \Omega \to \mathbb{R}$ of degree N that is determined by the *recovery conditions*

$$\mathcal{A}(\Omega_{l,r})R^N_{l,k}(\cdot,\bar{u}^l) = \bar{u}^l_r, \qquad r \in \mathcal{S}_{l,k}. \tag{5}$$

Here $\mathcal{S}_{l,k}$ is the *stencil* of the polynomial $R^N_{l,k}(x,\bar{u}^l)$. It denotes an index set on level l with as many indices as degrees of freedom for $R^N_{l,k}$. These indices correspond to a local neighborhood of the element $\Omega_{l,k}$ and they provide an *admissible configuration*, in the sense that (5) leads to a uniquely solvable $R^N_{l,k}$.

The reconstruction operators are then defined by piecing together these polynomial reconstructions. If the elements are mesh-cells, then

$$\mathcal{R}_l\bar{u}^l(x) = R^N_{l,k}(x;\bar{u}^l), \qquad x \in \Omega_{l,k}. \tag{6}$$

Notice that consistency follows from the fact that $\Omega_{l,k}$ belongs to $\mathcal{S}_{l,k}$.

Remark The linearity of $\mathcal{D}_l$ and the recovery conditions imply that the reconstruction process has polynomial exactness of degree N, i.e.

$$R^N_{l,k}(\cdot,\bar{p}^l) = p(\cdot) \qquad \forall p \in \mathcal{P}_N \quad \text{with} \quad \bar{p}^l = \mathcal{D}_l p. \tag{7}$$

The sequences $\{\mathcal{R}_l\}$, $\{\mathcal{D}_l\}$ are used to define prediction operators, P^l_{l+1} : $V_{l+1} \to V_l$, that compute fine grid values from coarse grid values. These are defined as $P^l_{l+1} = \mathcal{D}_{l+1}\mathcal{R}_l$, hence

$$\tilde{u}^{l+1}_r := (P^{l+1}_l\bar{u}^l)_r = \mathcal{A}(\Omega_{l+1,r})R^N_{l,k}(\cdot,\bar{u}^l), \quad r \in \mathcal{M}_{l,k}, \quad l \in \mathbb{N}_0\,. \tag{8}$$

The prediction errors, computed as

$$e^{l+1}_k := \bar{u}^{l+1}_k - \tilde{u}^{l+1}_k, \quad k \in J_{l+1},$$

contain the information in $\bar{u}^{l+1}$ which cannot be predicted from the coarser data $\bar{u}^l = D^l_{l+1}\bar{u}^{l+1}$ by the prediction scheme P^l_{l+1}. These errors represent, hence, the difference in information between consecutive resolution levels.

Clearly, the discrete sets $\bar{u}^{l+1}$ and $(\bar{u}^l = D^l_{l+1}\bar{u}^{l+1}, e^{l+1} = \bar{u}^{l+1} - P^{l+1}_l\bar{u}^l)$ are equivalent. However there is an inherent redundancy in the information contained in e^{l+1}. In fact $D^l_{l+1}e^{l+1} \equiv 0$, see [Har96], i.e.

$$(D^l_{l+1}e^{l+1})_k = \sum_{r\in\mathcal{M}_{l,k}} m^{l,0}_{k,r}e^{l+1}_r = 0, \qquad k \in J_l \tag{9}$$

A non-redundant two scale representation of $\bar{u}^{l+1}$, can be obtained by defining the *scale coefficients*, or *detail coefficients*, as the coordinates of the prediction error expressed in a basis of $\mathcal{N}(D^l_{l+1})$, the null space of D^l_{l+1}. In [DGM00], following the guidelines of the standard theory in wavelet-type multiscale decompositions, the authors resort to the concept of *stable completions* to provide a working definition of the scale coefficients.

Notice that for each $\Omega_{l,k}$ there are $\#\mathcal{M}_{l,k}$ non-independent prediction errors. Because of (9), these can be adequately represented by $\#\mathcal{M}_{l,k} - 1$ independent quantities: the *scale coefficients*. When $\mathcal{S}_{l,k}$ is chosen independently of k, one finds that

$$d_k^l = \sum_{r \in \mathcal{M}_{l,k}} m_{k,r}^{l,1} e_r^{l+1}, \qquad k \in \mathcal{J}_{l,k} \tag{10}$$

where $\mathcal{J}_{l,k}$ is an index set associated to $\Omega_{l,k}$ and such that $\#\mathcal{J}_{l,k} = \#\mathcal{M}_{l,k} - 1$.

A one-to-one two-scale representation of a data set $\bar{u}^{l+1}$ is obtained by considering $\bar{u}^l = D_{l+1}^l \bar{u}^{l+1}$ and d_k^l in (10).

Let $\bar{u}^L = \mathcal{D}_L u$ for $u \in \mathcal{F}$, where L is the index of a sufficiently fine mesh $\mathcal{G}_L$. Repeating the previous process for the grid hierarchy $\{\mathcal{G}_l\}_{l=0}^L$ we obtain a multi-scale decomposition of $\bar{u}^L$.

$$\begin{gathered} u^L \Leftrightarrow \{u^{L-1}, d^{L-1}\} \quad \cdots \Leftrightarrow \cdots \{u^0; d^0; d^1; \cdots \quad d^{L-1}\} = M u^L \\ \begin{array}{ccccccccc} u^L & \to & u^{L-1} & \to & u^{L-2} & \to & \ldots & \to & u^0 \\ & \searrow & d^{L-1} & \searrow & d^{L-2} & \searrow & \ldots & \searrow & d^0 \end{array} \end{gathered} \tag{11}$$

Let us consider $u \in \mathcal{F}$ and $\bar{u}^L = \mathcal{D}_L u$. Relations (1) and (8) lead to

$$e_r^{l+1} = \bar{u}_r^{l+1} - \tilde{u}_r^{l+1} = \left(\mathcal{D}_{l+1}(u - R_{l,k}^N(\cdot, \bar{u}^l))\right)_r, \qquad r \in \mathcal{M}_{l,k}. \tag{12}$$

Notice that for any $p \in \mathcal{P}_N$, (12) and (7) imply that for $r \in \mathcal{M}_{l,k} \subset J_{l+1}$

$$e_r^{l+1} = \mathcal{A}(\Omega_{l+1,r})(u - p) - \mathcal{A}(\Omega_{l+1,r}) R_{l,k}^N(\cdot, \mathcal{D}_l(u - p)). \tag{13}$$

Since smooth functions are well approximated by polynomials, the above relation shows that prediction errors are expected to be small in regions of smoothness. Because of (10) the same will hold for the scale coefficients d_k^l. It is precisely because of this relation that MR decompositions can be considered as a tool to adapt computational refinements to the local regularity of the solution.

In numerical simulations for time dependent HCLs, the starting point at each time step is a discrete data set $u^L = \{u_k^L\}_{k=1}^{J_L}$ so that each value u_k^L is linked to a particular *element* of an underlying mesh $\mathcal{G}_L$. The grid *elements* can be either mesh cells, as in standard finite volume schemes, but also mesh points as in the ENO numerical schemes considered in [SO88]. Within Harten's framework for MR, each interpretation (cell-averages or point-values) has an associated *natural* MR setting.

As an example, we briefly review next the point-value MR setting.

2.1 Interpolatory MR

In the point-value framework for MR the grid elements are the mesh nodes. In what follows, it will be convenient to be a bit more specific in our description. For this, we consider a sequence of uniform nested grids on $[0, 1]$ $\mathcal{G}_l = \{x_k^l\}_{k=0}^{J_l}$, obtained by recursive dyadic refinement of $\mathcal{G}_0$, which we consider as the coarsest resolution level associated to our underlying problem. Hence $\Omega_{l+1,2k} = x_{2k}^{l+1} = x_k^l = \Omega_{l,k}$ (see Fig. 2.1-left), $h_l = 2^{-l} h_0$, $J_l = 2^l J_0$.

Cartesian meshes in 2D or 3D are obtained by a tensor product construction using these 1D meshes, see Fig. 2.1-right (see e.g. [BH97] for more specific details). Within the Harten's general framework, the extension to unstructured meshes is conceptually straightforward, although its particular application requires a certain degree of familiarity with the technical aspects of using unstructured meshes for the solution of PDEs (see [AH98, Abg97] for specific details).

The transfer of information from fine to coarse is done by retaining those values attached to points in $\mathcal{G}^l \subset \mathcal{G}^{l+1}$ and discarding the rest. In the 1D case of Fig. 2.1-left, the *decimation by restriction* process is defined as $u_k^l = (D_{l+1}^l u^{l+1})_k = u_{2k}^{l+1}$. For the case 2D of Fig. 2.1-right $u_{k,m}^l = (D_{l+1}^l u^{l+1})_{k,m} = u_{2k,2m}^{l+1}$.

Decimation by restriction has a natural correspondence with the interpretation of the discrete sets as being the values of an underlying function $u(x)$ at the mesh points of each grid, i.e. if $\mathcal{D}_m u = u(\mathcal{G}_m)$, $\forall m$, then $u^l = D_{l+1}^l u^{l+1} = D_{l+1}^l \mathcal{D}_{l+1} u = u(\mathcal{G}_l) = \mathcal{D}_l u$.

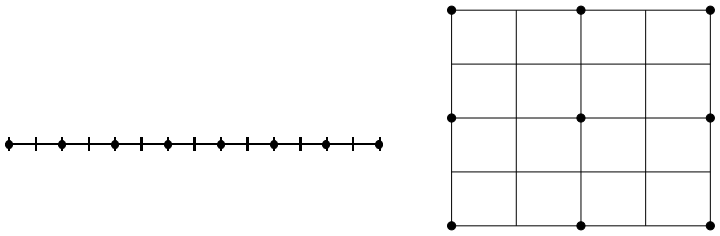

Fig. 1. +: mesh points in $\mathcal{G}^{l+1}$; •: Mesh points in $\mathcal{G}^l$. Left 1D, right 2D uniform meshes. Prediction errors are computed at points in $\mathcal{G}^{l+1} - \mathcal{G}^l$.

Given a grid element $x_k^l \in \mathcal{G}_l$, we consider the polynomial $L_{l,k}^N$ characterized by the recovery conditions

$$L_{l,k}^N(x_r^l; u^l) = u_r^l, \qquad r = k-p, \ldots, k+p+1 \tag{14}$$

where $p \geq 0$ is a fixed integer, chosen independently of l and k. Notice that $L_{l,k}^N(x; u^l)$ is the Lagrange interpolation polynomial of degree $N = 2p+1$ based on the stencil $\mathcal{S}_{l,k} = \{x_r^l\}_{r=k-p}^{k+p+1}$ and the data attached to it.

Following (6) we have (see also Fig. 2)

$$\mathcal{R}_l u^l(x) := L_{l,k}^N(x; u^l), \qquad x \in [x_k^l, x_{k+1}^l], \quad k = 0, \ldots J_l - 1 \tag{15}$$

and following (8) we get the *prediction* operator, which obtains fine data from coarse data, $\tilde{u}_m^{l+1} = (P_l^{l+1} u^l)_m = L_{l,[m/2]}^N(x_m^{l+1}, u^l)$. Hence

$$\tilde{u}_{2k}^{l+1} = L_{l,k}^N(x_{2k}^{l+1}, u^l) = L_{l,k}^N(x_k^l, u^l) = u_k^l \tag{16}$$

$$\tilde{u}_{2k+1}^{l+1} = L_{l,k}^N(x_{2k+1}^{l+1}, u^l) = \sum_{r=1}^{p} \beta_l (u_{k+r}^l + u_{k-r+1}^l) \tag{17}$$

where the coefficients β_m depend on N (see e.g. [Har96]).

Since $u_{2k}^{l+1} = u_k^l$, (16) implies that $e_{2k}^l = 0$. The prediction error for the odd values will not be zero in general, hence in this setting the scale coefficients are defined as $d_k^l := u_{2k+1}^{l+1} - \tilde{u}_{2k+1}^{l+1}$. The invertible two-scale transformation is ($k = 0, \ldots J_l - 1$)

$$\left\{ \begin{array}{l} u_k^l = u_{2k}^{l+1} \\ d_k^l = u_{2k+1}^{l+1} - \tilde{u}_{2k+1}^{l+1} \end{array} \right\} \quad \leftrightarrow \quad \left\{ \begin{array}{l} u_{2k}^{l+1} = u_k^l \\ u_{2k+1}^{l+1} = \tilde{u}_{2k+1}^{l+1} + d_k^l \end{array} \right\}. \tag{18}$$

Notice that the two discrete sets u^{l+1} and $\{(u^l, d^l)\}$, which have exactly the same cardinality, are absolutely equivalent.

The interpretation of a multiscale decomposition within the point-value setting is straightforward: The information contents of the sequence u^L, which is understood as the point-values of $u(x)$ on the (fine) grid $\mathcal{G}_L$, is decomposed as u^0, those same values but on a much coarser mesh plus a sequence of *scale* coefficients at each resolution level between $\mathcal{G}_0$ and $\mathcal{G}_L$. The scale coefficients d_k^l represent the difference in information between discretizations of the function at two consecutive resolution levels, or in other words, the information on level l that cannot be predicted from the coarse values one level below. In this framework the scale coefficients are simply interpolation errors.

Remark The centered-stencil construction for $L_{l,k}^N$ was used in [DD89] within the context of binary subdivision schemes, which were the basis of Donoho's construction of the Interpolatory Wavelet Transform (IWT) [Don92]. The IWT has been used to design adaptive schemes for scalar HCLs independently by Homlström [Hol99]

The relation between scale coefficients and smooth behavior. Let us assume that the discrete data $u^L = u(\mathcal{G}_L)$, where $u(x)$ is a piecewise smooth function. The scale coefficients in the point-value setting are simply interpolation errors, hence the relation between the behavior of the scale coefficients with respect to the regularity of u can be analyzed using elementary arguments in interpolation theory.

Figure 2 shows the piecewise polynomial interpolatory reconstruction (15) of a piecewise smooth function. We clearly observe that the quality of the approximation is degraded around the singularity, leading to large interpolation errors. Note that the region affected by the singularity is larger for higher degree polynomials.

A precise estimate of the size of the scale coefficients, can be given by expressing the error in Lagrange interpolation in its so-called *Newton form*

$$u(x) = L_{l,k}^N(x) + u[\mathcal{S}_{l,k}, x] w_{l,k}(x) \qquad x \in [x_k, x_{k+1}] \tag{19}$$

where $u[\mathcal{S}_{l,k}, x]$ denotes the $N+1$st divided difference of $u(x)$ at the points of the stencil and x and $w_{l,k}(x) = \Pi_{x_m^l \in \mathcal{S}_{l,k}}(x - x_m^l)$.

Since $d_k^l = u[\mathcal{S}_{l,k}, x_{2k+1}^{l+1}] w(x_{2k+1}^{l+1})$, the relation between the smoothness of a function and the behavior of the scale coefficients can be obtained by

Fig. 2. A piecewise smooth signal (solid line) and its point-values on a uniform grid (dots on solid line). Interpolatory reconstructions (Dotted lines). Left: $p = 1, N = 3$. Right $p = 2, N = 5$

considering the behavior of the divided differences with respect to singularities of the function. Let us assume that $u^{(s)}$ has a jump discontinuity in the convex hull of $\mathcal{S}_{l,k}$, while $u^{(m)}$ is smooth $0 \leq m < s$. Then it is shown in [Har95] that

$$d_k^l = 2^s d_{2k+i}^{l+1}, \qquad i = 0, 1.$$

Notice that the decay rate of the scale coefficients is intimately related to the smoothness of the underlying function and the uniform coarsening of the hierarchy of meshes. In particular, coefficients belonging to a region of smooth variation of $u(x)$ should approximately satisfy

$$d_k^l \approx 2^{N+1} d_{2k+i}^{l+1}, \qquad i = 0, 1 \tag{20}$$

so that any deviation from this behavior can be interpreted as lack of smoothness. This observation, which will be revisited later, lies at the heart of Harten's heuristics in designing adaptive multiresolution schemes for HCLs.

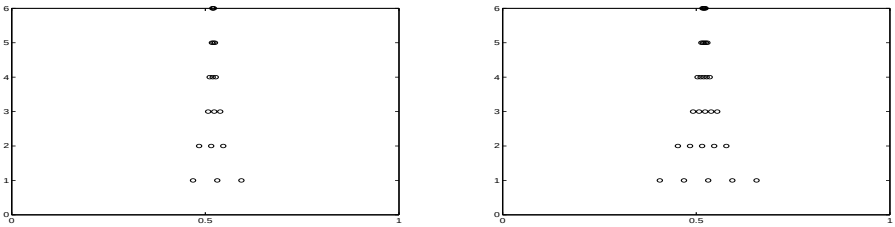

Fig. 3. Scale coefficients larger than 10^{-2} for the piecewise smooth signal of Fig. 2. Left: $p = 1$, $N = 3$. Right: $p = 2$, $N = 5$

2.2 Discretization by cell-averages

In finite volume formulations for HCL, the discrete numerical values are interpreted as approximations to the averages of the solution over the computational cells defined by the underlying grid. In this case it is more appropriate

to analyze the data within the *cell average framework*, in which the grid elements are the mesh-cells.

Given any locally integrable function $u(x) : \Omega \to \mathbb{R}$, the cell-average discretization operator is defined as

$$(\mathcal{D}_l u)_k = \mathcal{A}(\Omega_{l,k})u := \frac{1}{|\Omega_{l,k}|} \int_{\Omega_{l,k}} u(x)dx, \qquad k = 1, \ldots, J_l. \tag{21}$$

Notice that because of the additivity of the integral, relation (3) becomes

$$\bar{u}_k^l = (D_{l+1}^l u^{l+1})_k = \frac{1}{2}\left(\bar{u}_{2k}^{l+1} + \bar{u}_{2k+1}^{l+1}\right)$$

for the 1D meshes considered in the previous section and

$$(D_{l+1}^l \bar{u}^{l+1})_{k,j} = \frac{1}{4}\left(\bar{u}_{2k,2j}^{l+1} + \bar{u}_{2k+1,2j}^{l+1} + \bar{u}_{2k,2j+1}^{l+1} + \bar{u}_{2k+1,2j+1}^{l+1}\right) \tag{22}$$

for the 2D (tensor-product) extension.

The remaining ingredient in the MR transformation is the reconstruction process. The choice of centered stencils of mesh cells in 1D leads to MR transformations that are closely related to the biorthogonal wavelet framework (see e.g. [Har95, Coh03]). We refer the reader to [BH97] and [Got98] for specific descriptions related to our current application.

Relation between scale coefficients and smoothness. In 1D there is a natural relation between the cell-average and the interpolatory settings which can be exploited to give a simple proof that, for a given reconstruction of degree N, the scale coefficients in the MR representation also satisfy (20).

In Fig. 4 we observe that, as in the interpolatory case, the scale coefficients 'pile up' around the location of a jump discontinuity. The relation between scale coefficients and local regularity can be extracted by employing (13) (see [BH97, Got98] and also [Coh03]).

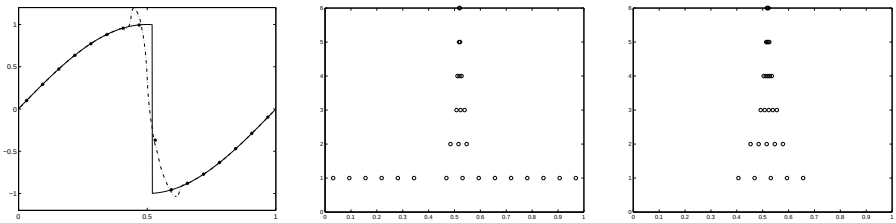

(a) (b) (c)

Fig. 4. (a) A piecewise smooth function (Solid line) and its cell-averages on a uniform grid (dots on solid line) . Polynomial reconstruction $p = 1$ (Dotted line); (b)-(c) Detail coefficients above $\epsilon_j = 10^{-2}/2^{7-j}$, $j = 1, \ldots, 6$. (b) $p = 1$, (c) $p = 2$

3 Multiresolution schemes within Harten's framework

We give next a brief 1D description of the basic strategy used in MR schemes for multidimensional computations.

Let us consider a conservative discretization of a 1D system of conservation laws

$$u_t + F(u)_x = 0 \tag{23}$$

which can be written as

$$U_k^{n+1} = U_k^n - \frac{\delta_t}{\delta_x} B(U^n)_k. \tag{24}$$

Conservativity means that the numerical divergence $B(U^n)_k$ has the form

$$B(U^n)_k = F(U^n_{k-s-1}, \ldots, U^n_{k+s}) - F(U^n_{k-s,\ldots,k+s+1}) \tag{25}$$

where the function $F(w_1, w_2, \ldots, w_{2s+1})$ is the numerical flux function.

Let M be a linear MR transformation based on a hierarchical set of computational meshes $\{\mathcal{G}_l\}_{l=0}^L$ on the domain of interest. Let us consider (24) on the finest mesh (the reference mesh) and denote the numerical values at time t_n as $U^n_{L,k}$. Since M is a linear transformation, we can write

$$MU^{n+1}_{L,k} = MU^n_{L,k} - \lambda_L M B^n_{L,k} \tag{26}$$

with $\lambda_L = \delta_t / h_l$ and $B^n_{L,k} = B(U^n_L)_k$

Harten's development of multiresolution schemes for HCLs was tightly linked to previous work on Essentially Non Oscillatory (ENO) schemes, a class of HRSC schemes for HCLs that obtain very good resolution properties by performing an elaborate, but very costly, computation of the numerical flux functions at cell interfaces. With the aim of reducing the cost inherent to such schemes, in [BH95, BH97] the authors concentrate on the idea of eliminating heavy flux computations wherever the multiscale analysis reveals that the solution is smooth. This cost-reduction alternative was further explored in different contexts, e.g. [Abg97, Bih96, BOLR01] and the work of the first two authors [CD01, CDM01, RCD03]. In section 3.1 we outline the implementation in [CD01].

Starting with the work in [GM99], a parallel development seeks to perform the time evolution of the numerical values only for a locally refined grid determined from the smoothness information contained in the MR decomposition of the numerical data at the beginning of the time step [Mül02, CKMP03]. In section 3.2 we describe the essential features of this development.

These are two options that lead to essentially different MR-based adaptive schemes for HCL. They both evolved from Harten's original MR-based adaptive concept and share several common ingredients:

The multiresolution transform. The choice of M is dictated by the interpretation of the numerical values. Hence, MR transformations within the

cell-average framework are used for the finite-volume schemes considered in [BH95, BH97, Abg97, Bih96, BOLR01] and also in [GM99, Mül02, CKMP03].

Following the work in [SO88], many state of the art HRSC schemes in conservation form consider the numerical values as approximations to the point-values of the solution. This simplifies the implementation on Cartesian meshes in 2D and 3D and was the main motivation in [CD01] for considering the point-value framework as the appropriate multiresolution framework.

The thresholding algorithm. A key point lies in the analysis of the local regularity of *both* U^n and U^{n+1}, where the latter is of course unknown at time n, and how this information is used within the adaptive scheme.

The user introduces a *thresholding parameter* ε, which controls the difference between the reference simulation (the numerical values on the finest grid) and the outcome of the multilevel computation.

Given U_L^n and $MU_L^n = (U_0^n, d^1(U^n), \dots d^L(U^n))$, the set of indices of *significant coefficients* is constructed as

$$\mathcal{D}_{L,\epsilon}^n := \left\{(l,k)\ ;\ |d_k^l(U^n)| > \varepsilon_l,\ k \in J_l,\ l \in \{0,\dots,L-1\}\right\} \tag{27}$$

where ε_l is a level-dependent threshold value related to ε. This set identifies those locations where the prediction operator produces large errors, hence it is related to locations where data U_L^n display non-regular behavior.

In practice $\varepsilon_l = \varepsilon\ \forall l$ in the point-value framework and $\varepsilon_{L-1} = \varepsilon$, $\varepsilon_l = \varepsilon_{l+1}/2$, $l < L-1$ in the cell-average framework. This choice is motivated by the stability properties of M^{-1}. We refer the interested reader to [Har96].

The prediction step. The corresponding set for U_L^{n+1}, i.e. $\mathcal{D}_{L,\epsilon}^{n+1}$, is also needed for the design of the adaptive strategy, but since U_L^{n+1} is not known at the beginning of the time step, we can only give an *estimation*, $\tilde{\mathcal{D}}_{L,\epsilon}^{n+1}$, which is computed so that

$$\mathcal{D}_{L,\epsilon}^n \cup \mathcal{D}_{L,\epsilon}^{n+1} \subset \tilde{\mathcal{D}}_{L,\epsilon}^{n+1}, \tag{28}$$

To compute the set $\tilde{\mathcal{D}}_{L,\epsilon}^{n+1}$, which marks the non-smooth regions of *both* U_L^n and U_L^{n+1}, all implementations of MR-based schemes known to us employ Harten's heuristic approach: In solving HCLs there are two effects that have to be taken into account: Finite speed of propagation and compressibility (i.e. convergence of characteristics which is ultimately responsible for the creation of shock waves). If a singularity is formed, the CFL condition of the underlying scheme will limit its speed of propagation. If compression mechanisms are steepening up a numerical profile, this should be detected as a loss of local regularity in the behavior of the scale coefficients.

Based on the results of section 2.1 Harten's heuristics for the computation of $\tilde{\mathcal{D}}_{L,\epsilon}^{n+1}$ in 1D proceeds as follows:

$$\begin{aligned} \text{if } (l,k) \in \mathcal{D}_{L,\epsilon}^n &\implies (l,k-i) \in \tilde{\mathcal{D}}_{L,\epsilon}^{n+1} \quad i = -2,..,2 \\ \text{if } |d_k^l| \geq 2^{N+1}\epsilon_l \text{ and } l < L &\implies (l+1,2k+i) \in \tilde{\mathcal{D}}_{L,\epsilon}^{n+1} \quad i = -1,0,1 \end{aligned}$$

The first test takes into account the propagation of information (recall that the propagation of 'real' information is limited by the CFL condition). The second one aims at detecting shock formation. In a smooth region the local rate of decay of the detail coefficients is determined by the accuracy of the interpolation and the local regularity of the function. The second test measures whether the decay rate is that of a smooth function, if this is not the case, compression leading to shock formation might be taking place and the location is also marked.

To the best of our knowledge, Harten's heuristic strategy has not been rigorously verified to satisfy condition (28). In [CKMP03] the authors are able to give a theoretical justification of (28) for a slight modification of Harten's heuristics. For this modification, the reliability of the adaptive scheme is fully ensured, since (28) guarantees that no significant future feature of the solution is missed. In practice, however, Harten's heuristics seems to be sufficient.

3.1 Cost-Effective Multiresolution schemes for shock computations

State of the art HRSC schemes succeed in computing highly accurate numerical solutions, (third order or higher) in regions of smoothness, while maintaining at the same time sharp, oscillation free, numerical profiles at discontinuities. These desirable features are achieved by performing a specific, and often very expensive, computation of the numerical flux functions at each cell boundary.

When the underlying grid is uniform, the implementation of these shock capturing schemes is quite straightforward. Fine grid simulations with HRSC schemes render very precise numerical approximations to the solution of HCLs, but the heavy-duty flux computations increase the computational cost in such a way that for some HRSC schemes 2D fine mesh simulations on personal computers are out of reach simply because they cost too much.

It is common knowledge that the high-powered flux computations involved in these schemes are only strictly needed at existing singularities or when these are about to form. Hence, if *both* U^n and U^{n+1} are smooth around a specific location on the underlying computational mesh, it means that no singularity is present or will be created in the course of the computation, hence we could avoid using the numerical flux functions of the HRSC scheme in the computation of the numerical divergence at that location. On the other hand, around a discontinuity (or when a steep gradient makes it imminent), the full power of the HRSC scheme is needed, if the high-resolution properties of the scheme are to be maintained.

This observation forms the basis of the cost-effective alternative: The goal is to substitute the direct (HRSC) computation of the numerical divergence on the finest mesh by a multilevel computation based on the smoothness information obtained from the MR transformation M. The basic *cost-reduction* assumption is that interpolating numerical divergences is considerably faster than computing the necessary fluxes.

The cost-reduction alternative involves no memory savings. However, and precisely because of this feature, there is no need for special data structures and the necessary MR modules can be easily incorporated into any existing CFD code. When memory requirements are not a major concern (as it is the case in many 2D computations), this technique often provides the necessary *cost-reduction* factors to allow very fine HRSC simulations on personal computers [CD01, RCD03].

The boolean flag. Thresholding and prediction, as described in the previous section, are combined so that the set $\tilde{\mathcal{D}}_L^{n+1}$ is converted into the determination of a boolean flag whose value, 0 or 1, will determine the choice of procedure to compute the numerical divergence.

For a given tolerance parameter ϵ, starting from a zero value for all b_k^l, one applies for each detail coefficient the following two tests:

$$\text{if } |d_k^l| \geq \epsilon_l \implies b_{k-i}^l = 1 \quad i = -2, .., 2$$
$$\text{if } |d_k^l| \geq 2^{N+1}\epsilon_l \text{ and } l < L \implies b_{2k+i}^{l+1} = 1 \quad i = -1, 0, 1$$

In the point-value setting, the extension to 2D is straightforward (see [CD01]). For the cell-average framework see [BH95, DGM00].

The multilevel evaluation of the numerical divergence within the point-value setting. Instead of computing B_L^n with the HRSC scheme at all points in $\mathcal{G}_L$, in [CD01] we apply the following procedure involving the boolean flags defined previously

1) Compute B_0^n (*i.e* for all points of the coarsest grid $\mathcal{G}_0$) directly with the HRSC scheme.
2) Repeat for $l = 0$ to $L-1$ to obtain B_L^n:
   For each $x_{2k+1}^{l+1} \in \mathcal{G}_{l+1} - \mathcal{G}_l$:
   - if $b_k^l = 1$ the location is flagged as non-smooth, so that a precise computation of the numerical divergence is required: Compute $B_{l+1,2k+1}^n$ directly with the HRSC scheme.
   - if $b_k^l = 0$ the location belongs to a smooth region and a direct (expensive) computation can be avoided: Compute $B_{l+1,2k+1}^n$ using the prediction operator in M, i.e. $B_{l+1,2k+1}^n = (P_l^{l+1} B_l^n)_{2k+1}$.

The cpu gain of this algorithm lies in the fact that the cost of the prediction operator is negligible compared to the expensive HRSC evaluation.
As an example, in our implementation for the 2D Euler equations [CD01], the prediction operator is based on a 2D Lagrange polynomial interpolation of degree 3 (see [BH97]) and we use a (formally) third order HRSC described in [DM96] for which the effective ratio for the evaluation of one numerical divergence is about 1/100.
Remark: Since the grids $\{\mathcal{G}_l\}_l$ are embedded, and the numerical values are attached to mesh points in the point-value setting, each direct (HRSC) evaluation must be done with the values of U^n on the finest grid $\mathcal{G}_L$ (they are

always available in this method). This guarantees that the numerical divergence is *always* computed by the HRSC with a precision related to the *finest* spatial discretization step.

This multilevel strategy has been detailed, analyzed and tested on several benchmark tests involving the 2D Euler equations. Numerical results, which are reported in a series of papers [CD01, CDM01, RCD03], indicate that the quality of the multilevel approximation (the difference between the outcome of the multilevel algorithm and the reference simulation) is directly controlled by the tolerance parameter ϵ used in the thresholding algorithm.

The efficiency of the multilevel scheme is, of course, problem dependent. We refer again to the aforementioned papers for a specific evaluation of the efficiency of the multilevel scheme in several situations. Here we present a specific simulation that illustrates its performance. We have represented on Fig. 8 the result of the interaction between a Taylor vortex and a Mach 4 shock. This interaction is difficult to handle numerically for Mach numbers larger than 2, where the use of robust HRSC methods are necessary in order to represent correctly the physics of the problem. Using the multilevel method outlined in this section, we performed in [RCD03] a detailed study of the phenomenology of these interactions.

The parameters used for the simulation in Fig. 8 are the following: The computational domain is $[0,1]\times[0,2]$, the finest grid $\mathcal{G}_L$ has 512×256 uniformly spaced points and the coarsest $\mathcal{G}_0$ is 8×4 points (6 levels of refinement). The thresholding parameter is $\epsilon = 5.10^{-4}$. We display a numerical Schlieren plot of the density at times $t = 0$ and $t = 0.4$. Associated to each density plot we show a display where only the points for which the numerical divergence has been evaluated by the HRSC scheme are represented.

After the interaction the flow becomes much more complex, the vortex is highly distorted and a strong acoustic wave develops ahead of it. All these features are correctly identified by the adaptive strategy, which validates the smoothness analysis done by the wavelet coefficients.

In this simulation, the percentage of points where a direct evaluation is done grows only from 3.4% to 10.6%, leading to an effective cpu time reduction of a factor **6.8** compared to a reference simulation without the multilevel strategy.

3.2 Fully Adaptive Finite Volume Schemes

A modified approach has been developed that is aiming at reducing the computational costs with regard to both computational time *and* memory requirements but still maintaining the accuracy of the reference scheme. The main idea is to evolve in time only the cell averages of a *locally refined grid*, so that the finest (reference) mesh does not need to be available.

We emphasize that the ultimate goal is to provide an algorithm that can be realized with an optimal complexity, i.e., the number of floating point operations is proportional to the number of cells in the adaptive grid. This

requires new data structures supporting the local structure of the algorithm. Here *hash tables* turned out to be a very efficient tool. For details on the implementation and the realization of the algorithms in terms of these data structures we refer to [MV00]. Tree structures have also been considered in [RSTB03]

In the following we summarize the main ingredients specific to this *fully adaptive* concept, namely, *local grid refinement* and *evolution of local cell averages*. For more specific details we refer to [Mül02].

Local Grid Refinement

The starting point is a locally refined grid characterized by the index set $\mathcal{G}^n_{L,\epsilon} \subset \{(l,k)\,;\, k \in J_l,\ l = 0,\ldots,L\}$ such that

$$\Omega = \bigcup\nolimits_{(l,k)\in\mathcal{G}^n_{L,\epsilon}} \Omega_{l,k}.$$

that is provided with cell averages $\{U^n_{l,k}\}_{(l,k)\in\mathcal{G}_{L,\epsilon}}$ corresponding to time step n. It is required that the set $\mathcal{G}^n_{L,\epsilon}$ has the structure of a graded tree.

We will now summarize the six steps of the local grid refinement procedure in the context of cell averages, namely, (i) *local MR transformation*, (ii) *thresholding*, (iii) *prediction*, (iv) *grading*, (v) *local grid refinement* and (vi) *local inverse MR transformation*.

Local MR transformation. As outlined in sections 2 and 2.2 we perform a MR analysis of the cell averages at hand which provides a new data format composed of data on a coarsest discretization level and arrays of details describing the difference information between the data on two consecutive discretization levels. For this purpose we proceed level by level from fine to coarse as indicated in (11). Note that the two-scale transformation is performed locally only for the indices corresponding to the adaptive grid instead of the full levels. In particular, applying the local two-scale transformation can be interpreted as a successive coarsening of the grid where fine-grid cells are agglomerated to a coarse-grid cell and the difference information is stored by the detail coefficients.

Thresholding. We now apply a hard thresholding to the sequence of detail coefficients, i.e., discard all details d^l_k that fall in absolute value below a certain threshold value. Here we apply the same strategy as in section 3. For this purpose we compute the index set $\mathcal{D}^n_{L,\epsilon}$ corresponding to the *significant details* according to (27).

Prediction. To perform the evolution step, we have to determine the adaptive grid on the *new* time level. Therefore we *predict* all significant details on time level $n+1$ that may become significant due to the evolution. In practice, we use Harten's heuristic strategy summarized in section 3 to compute the prediction set $\tilde{\mathcal{D}}^{n+1}_{L,\epsilon}$.

Grading. In order to perform the grid adaptation procedure level by level we need that the index set of significant details corresponds to a *graded tree*,

i.e., the levels of neighboring cells differ at most by one. Since the set $\tilde{\mathcal{D}}_{L,\epsilon}^{n+1}$ is in general not graded, we have to apply in addition a grading procedure. This will slightly inflate the index set of significant details but has so far been observed not to spoil the complexity reduction of floating point operations in any significant way. In fact, from the nature of singularities occurring in flow computations one expects the distribution of significant details to exhibit at least nearly tree structure (see figures 3, 4).

Grid adaptation. Then we exploit the inflated set $\tilde{\mathcal{D}}_{L,\epsilon}^{n+1}$ to determine an associated index set $\mathcal{G}_{L,\epsilon}^{n+1}$ which characterizes the adaptive grid at the new time level. The index set $\mathcal{G}_{L,\epsilon}^{n+1}$ is initialized by all indices of the coarsest discretization. Then, traversing through the levels from coarse to fine we proceed as follows: if $(l,k) \in \tilde{\mathcal{D}}_{L,\epsilon}^{n+1}$ then the cell $\Omega_{l,k}$ is locally refined, i.e., the index (l,k) is removed from $\mathcal{G}_{L,\epsilon}^{n+1}$ and the indices of the subcells on the finer level are added to $\mathcal{G}_{L,\epsilon}^{n+1}$. Finally we obtain the locally adapted grid which naturally corresponds to the leaves of the graded tree of significant details.

Local inverse MR transformation By the previous step the grid has locally changed due to local refinement and coarsening. In order to determine the cell averages $\{U_{(l,k)}^n\}_{(l,k)\in\mathcal{G}_{L,\epsilon}^{n+1}}$, we employ a local inverse MR transformation interrelating the local cell averages $(U_{l,k}^n)_{(l,k)\in\mathcal{G}_{L,\varepsilon}^n}^n$ and the significant details $(d_k^l)_{(l,k)\in\mathcal{D}_{L,\varepsilon}^n}$. Again we proceed level by level from coarse to fine where we locally replace a cell average on the coarse scale by the cell averages of its subcells whenever there is a significant detail associated to this coarse cell in $\tilde{\mathcal{D}}_{L,\epsilon}^{n+1}$. Note that the computation of these cell averages can be simultaneously determined when performing the grid adaptation.

Evolution of Local Cell Averages

The time evolution of the cell averages is now performed on the new adaptive grid determined by the index set $\mathcal{G}_{L,\epsilon}^{n+1}$

$$U_{l,k}^{n+1} = U_{l,k}^n - \lambda_l \, B_{l,k}^n, \quad \lambda_{l,k} := \frac{\delta\, t}{|\Omega_{l,k}|} \qquad (l,k) \in \mathcal{G}_{L,\epsilon}^{n+1}, \tag{29}$$

where $B_{l,k}^n$ denotes the numerical divergence of cell $\Omega_{l,k}$.

In principle, the adaptive grid could be interpreted as an unstructured grid and the numerical divergence could be computed by the local data at hand, see for instance [RSTB03]. Since the ultimate goal is the design of an adaptive scheme with an error still corresponding to the discretization of the *finest* grid, this strategy could result in a severe accuracy deficiency. Therefore we have to be more careful in the computation of the local numerical divergence. For this purpose, we assume that a reference FVS is given on the uniform finest grid $\mathcal{G}_L$ similar to (29) with the numerical divergence

$$B_{L,k}^n := \sum\nolimits_{\Gamma_{k,r}^L \subset \partial\Omega_{L,k}} |\Gamma_{k,r}^L| \, F_{k,r}^{L,n}$$

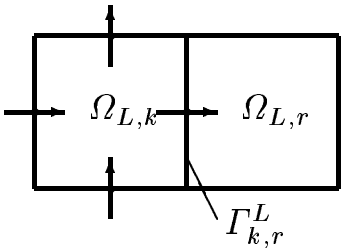

Fig. 5. Finite volume discretization

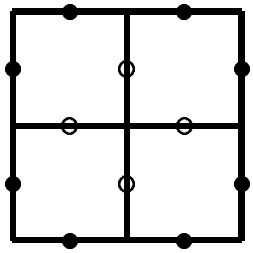

Fig. 6. Local flux balances, (•) boundary flux, (∘) internal flux

determined by the sum of all fluxes over all cell edges of the cell $\Omega_{L,k}$. Here $\Gamma^L_{k,l}$ denotes the interface of the cell $\Omega_{L,k}$ to the neighbor cell $\Omega_{L,r}$ and $F^{L,n}_{k,r}$ the corresponding numerical flux. See Fig. 5 for clarification of notation. The numerical fluxes are assumed to be conservative, i.e.,

$$F^{L,n}_{k,r} = -F^{L,n}_{r,k}. \tag{30}$$

Applying (virtually) the linear MR transformation M for cell averages similar to (26) results in local evolution equations for the cell averages on the coarser scales $l = 0, \ldots, L-1$, see (29), where the local numerical divergence is recursively defined by

$$B^n_{l,k} := \sum\nolimits_{\Omega_{l+1,r} \subset \Omega_{l,k}} B^n_{l+1,r}. \tag{31}$$

This is sketched in Fig. 6 for a dyadic grid refinement. According to (31) we have to compute all fluxes marked by • and ∘. However, the internal fluxes corresponding to ∘ cancel each other out due to the conservation property (30) resulting in a significant reduction of the computational complexity. Finally, we end up with

$$B^n_{l,k} = \sum\nolimits_{\Gamma^l_{k,r} \subset \partial\Omega_{l,k}} |\Gamma^l_{k,r}|\, F^{l,n}_{k,r} \tag{32}$$

where the local numerical fluxes are defined by

$$F^{l,n}_{k,r} := \sum\nolimits_{\Gamma^{l+1}_{j,s} \subset \Gamma^l_{k,r}} \frac{|\Gamma^{l+1}_{j,s}|}{|\Gamma^l_{k,r}|} F^{l+1,n}_{j,s} = \sum\nolimits_{\Gamma^L_{j,s} \subset \Gamma^l_{k,r}} \frac{|\Gamma^L_{j,s}|}{|\Gamma^l_{k,r}|} F^{L,n}_{j,s}. \tag{33}$$

Together with (29) this specifies the fully adaptive scheme. Note that we never employ the complexity of the finest grid.

Remark. In 1D the local flux computation simplifies because there are no hanging nodes in the adaptive grid. Due to the nestedness of the grids, see Fig. 2.1, the numerical fluxes on level l coincide with the numerical fluxes on the higher scales, i.e.,

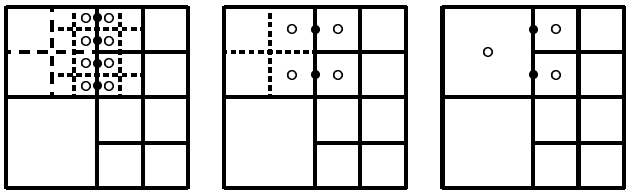

Fig. 7. Exact (left), locally structured (middle) and unstructured (right) flux computation, (•) numerical flux, (∘) cell average

$$F^n_{l,k} = F^n_{l+1,2k} = \ldots = F^n_{L,2^{L-l}k} \equiv F(U^n_{L,2^{L-l}k-s,\ldots,2^{L-l}k+s+1}). \tag{34}$$

Since the numerical divergence on the coarser levels is recursively defined we further conclude

$$B^n_{l,k} := B^n_{l,2k} + B^n_{l,2k+1} = \sum_{i=0}^{2^{L-l}-1} B^n_{L,2^{L-l}k+i} = F^n_{L,2^{L-l}(k+1)} - F^n_{L,2^{L-l}k}.$$

Remark. According to (33) the numerical fluxes have to be computed by the data on the *finest* scale. In order to provide these data we have to perform locally an inverse two-scale transformation. In 1D this does not degrade the complexity of the algorithm but it will in higher space dimensions. For HRSC we may perform the local flux computation by means of the local data at hand instead of the data on the finest scale, see Fig. 7 (middle and right). In practice, this does not affect the accuracy but preserves the computational complexity. In this case, the number of flux computations is proportional to the number of significant detail coefficients $\#\mathcal{D}^n_{L,\epsilon}$ or $\#\mathcal{G}^n_{L,\epsilon}$, respectively.

Remark. In Harten's original approach [Har95, BH97], the complexity is not reduced. To see this, we consider Fig. 6. Here expensive fluxes based on higher–order upwind discretizations are computed at • and, in addition, cheap finite difference flux approximations have to be computed at ∘.

Data Structures, Error Control and Real World Applications

In the previous section we outlined an adaptive MR scheme with an optimal complexity in the sense that the number of operations is proportional to the number of unknowns, i.e., $\#\,\mathcal{D}_{L,\epsilon}$ and $\#\,\mathcal{G}_{L,\epsilon}$, respectively. In order to design an *optimal* code, i.e., the memory requirements and the CPU time are proportional to the complexity of the adaptive algorithm, it turns out that the choice of the *data structures* and the *memory management* has a significant influence on the performance of the computation. In particular, the design of appropriate data structures crucially depends on the underlying adaptive algorithm, i.e., the data structures have to be adapted to the algorithmic requirements and should not be designed independently. For our purposes the

concept of *hashing* turns out to be an efficient tool. To this end, we developed the template library `igpm_t_lib`, see [MV00], from which we derive the appropriate data structures for the realization of the adaptive code.

Concerning the quality of the computation we are aiming at the accuracy of the reference scheme. For this purpose, the local data provided by the adaptive scheme are projected onto the finest mesh applying the inverse MR transformation where the non-significant details are put to zero. The ideal strategy would be to determine the threshold value ϵ such that the *discretization error* of the reference scheme, i.e., difference between exact solution and reference scheme, and the *perturbation error*, i.e., the difference between the reference scheme and the adaptive scheme, are balanced. For scalar conservation laws this concept was rigorously verified, see [CKMP03].

By now the new adaptive MR concept has been applied by several groups with great success to different real world applications, e.g., 2D/3D–steady state computations of compressible fluid flow around air wings modeled by the Euler and Navier–Stokes equations, respectively, as well as fluid-structure interactions on block–structured curvilinear grid patches [BGMH$^+$03, BLM03], non–stationary shock–bubble interactions on 2D Cartesian grids for Euler equations [Mül02], backward–facing step on 2D triangulations [CKP02] and simulation of a flame ball modeled by reaction–diffusion equations on 3D Cartesian grids [RSTB03].

An example is shown for the transonic flow over a NACA0012 airfoil at $M_\infty = 0.95$, $\alpha = 0°$, see figures 9 and 10. The flow pattern downstream of the trailing edge is characterized by a complex shock configuration frequently referred to as *fish-tail*. The oblique shocks extend about 10 to 12 chord lengths into the flow domain. The steady–state computation was carried out using an implicit local–time stepping using the QUADFLOW solver [BGMH$^+$03]. The final adaptive grid consists of 55084 cells which provides a very high resolution over the complete extent of the shocks. Such a high shock resolution is not feasible using standard structured grids. Discretization of the shock region only by a uniform structured mesh equals about $29.5 \cdot 10^6$ grid cells. A uniform discretization of the complete flow domain would result in about 10^8 cells.

4 Conclusion

Harten's early developments on the use of MR techniques for numerical computations involving HCLs were presented as an attractive alternative to the adaptive grid methodology. The schemes currently in use show that the MR decomposition of the numerical data at each time step provides an adequate tool to adapt the computational resources to the nature of the data.

Cost-effective MR-based schemes provide an easy to use adaptive tool that has been succesfully used to investigate the behavior of new HRSC schemes. Fully adaptive MR-based schemes become a novel AMR technique, where the

refinement criteria is based on the smoothness information contained in the MR representation of the data.

Acknowledgements: Research supported by EU financed networks no. HPRN-CT-2002-00282 and no. HPRN-CT-2002-00286. The second author acknowledges partial support from Spanish MCYT-BFM2001-2814.

References

[Abg97] R. Abgrall. Multiresolution analysis on unstructured meshes: Applications to CFD. In Chetverushkin et al., editor, *Experimentation, modelling and computation in flow, turbulence and combustion.* John Wiley & Sons, 1997.

[AH98] R. Abgrall and A. Harten. Multiresolution representation in unstructured meshes. *SIAM J. Num. Anal.*, 35-6:2128–2146, 1998.

[BC89] M. Berger and P. Colella. Local adaptive mesh refinement for shock hydrodynamics. *Journal of Comput. Phys.*, 82:64–84, 1989.

[BGMH+03] F. Bramkamp, B. Gottschlich-Müller, M. Hesse, Ph. Lamby, S. Müller, J. Ballmann, Brakhage K.-H. and Dahmen W. *H*-adaptive Multiscale Schemes for the Compressible Navier–Stokes Equations — Polyhedral Discretization, Data Compression and Mesh Generation. In J. Ballmann, editor, *Flow Modulation and Fluid-Structure-Interaction at Airplane Wings*, volume 84 of *Numerical Notes on Fluid Mechanics*, pages 125–204. Springer, 2003.

[BH95] B. Bihari and A. Harten. Application of generalized wavelets: An adaptive multiresolution scheme. *J. Comp. Appl. Math*, 61:275–321, 1995.

[BH97] B. Bihari and A. Harten. Multiresolution schemes for the numerical solution of 2–D conservation laws I. *SIAM J. Sci. Comput.*, 18(2):315–354, 1997.

[Bih96] B. Bihari. Multiresolution schemes for conservation laws with viscosity. *J. Comp. Phys.*, 123:207–225, 1996.

[BLM03] F. Bramkamp, Ph. Lamby, and S. Müller. An adaptive multiscale finite volume solver for unsteady and steady state flow computations. 2003. submitted for publication.

[BMP92] E. Bacry, S. Mallat, and G. Papanicolaou. A wavelet based space-time adaptive numerical method for partial differential equations. *Mathematical Modeling and Numerical Analysis*, 26(7):793, 1992.

[BO84] M. Berger and J. Oliger. Adaptive mesh refinement for hyperbolic partial differential equations. *J. of Comput. Phys.*, 53:484–512, 1984.

[BOLR01] B.L. Bihari, D.K. Ota, Z. Liu, and S.V. Ramakrishnan. The multiresolution method on general unstructured meshes. *AIAA paper*, (AIAA 2001-2553), 2001.

[CD01] G. Chiavassa and R. Donat. Point value multiresolution for 2D compressible flows. *SIAM J. Sci. Comput.*, 23(3):805–823, 2001.

[CDKP00] A. Cohen, N. Dyn, S.M. Kaber, and M. Postel. Multiresolution finite volume schemes on triangles. *J. Comp. Phys.*, 161:264–286, 2000.

[CDM01] G. Chiavassa, R. Donat, and A. Marquina. Fine-mesh numerical simulations for 2d Riemann problems with a multilevel scheme. In

H. Freistühler and G. Warnecke, editors, *Hyperbolic Problems: Theory, Numerics, Applications*, pages 247–256. Birkhäuser, 2001.

[CKMP03] A. Cohen, S.M. Kaber, S. Müller, and M. Postel. Fully Adaptive Multiresolution Finite Volume Schemes for Conservation Laws. *Math. Comp.*, 72(241):183–225, 2003.

[CKP02] A. Cohen, S.M. Kaber, , and M. Postel. Multiresolution Analysis on Triangles: Application to Gas Dynamics. In G. Warnecke and H. Freistühler, editors, *Hyperbolic Problems: Theory, Numerics, Applications*, pages 257–266. Birkhäuser, 2002.

[Coh03] A. Cohen. Numerical Analysis of wavelet Methods. Studies in Mathematics and its Applications, 32. North-Holland-Elsevier, Amsterdam, 2003.

[Dah97] W. Dahmen. Wavelet and multiscale methods for operator equations. *Acta Numerica*, 6:55–228, 1997.

[DD89] G. Deslauries and S. Dubuc. Symmetric iterative interpolation processes. *Constructive Approximation*, 5:49–68, 1989.

[DGM00] W. Dahmen, B. Gottschlich–Müller, and S. Müller. Multiresolution schemes for conservation laws. *Numer. Math.*, 88(3):399–443, 2000.

[DM96] R. Donat and A. Marquina. Capturing shock reflections: An improved flux formula. *J. Comp. Phys.*, 125(1):42–58, 1996.

[Don92] D. Donoho. Interpolating wavelet transforms. Technical Report 408, Dept. of Statistics, Stanford University, 1992.

[GM99] B. Gottschlich–Müller and S. Müller. Adaptive finite volume schemes for conservation laws based on local multiresolution techniques. In M. Fey and R. Jeltsch, editors, *Hyperbolic Problems: Theory, Numerics, Applications*. Birkhäuser, 1999.

[Got98] B. Gottschlich–Müller. *On Multiscale Concepts for Multidimensional Conservation Laws*. PhD thesis, RWTH Aachen, October 1998.

[Har95] A. Harten. Multiresolution algorithms for the numerical solution of hyperbolic conservation laws. *Comm. Pure Appl. Math.*, 48(12):1305–1342, 1995.

[Har96] A. Harten. Multiresolution representation of data: A general framework. *SIAM J. Numer. Anal.*, 33(3):1205–1256, 1996.

[Hol99] M. Holmström. Solving hyperbolic pdes using interpolatory wavelets. *SIAM J. Sci. Comput.*, 21-2:405–420, 1999.

[LT] J. Liandrat and P. Tchamitchian. Resolution of the 1d regularized burgers equation using a spatial wavelet approximation. ICASE Report 90-83.

[Mül02] S. Müller. *Adaptive Multiscale Schemes for Conservation Laws*, volume 27 of *Lecture Notes on Computational Science and Engineering*. Springer, 2002.

[MV00] S. Müller and A. Voss. A Manual for the Template Class Library `igpm_t_lib`. IGPM–Report 197, RWTH Aachen, 2000.

[RCD03] A. Rault, G. Chiavassa, and R. Donat. Shock-vortex interactions at high mach numbers. *J. Scientific Computing*, 19:347–371, 2003.

[RSTB03] O. Roussel, K. Schneider, A. Tsigulin, and H. Bockhorn. A conservative fully adaptive multiresolution algorithm for parabolic PDEs. *J. Comp. Phys.*, 188(2):493–523, 2003.

[SO88] C.-W. Shu and S. Osher. Efficient implementation of essentially non–oscillatory shock capturing schemes I. *J. Comp. Phys.*, 77:439–471, 1988.

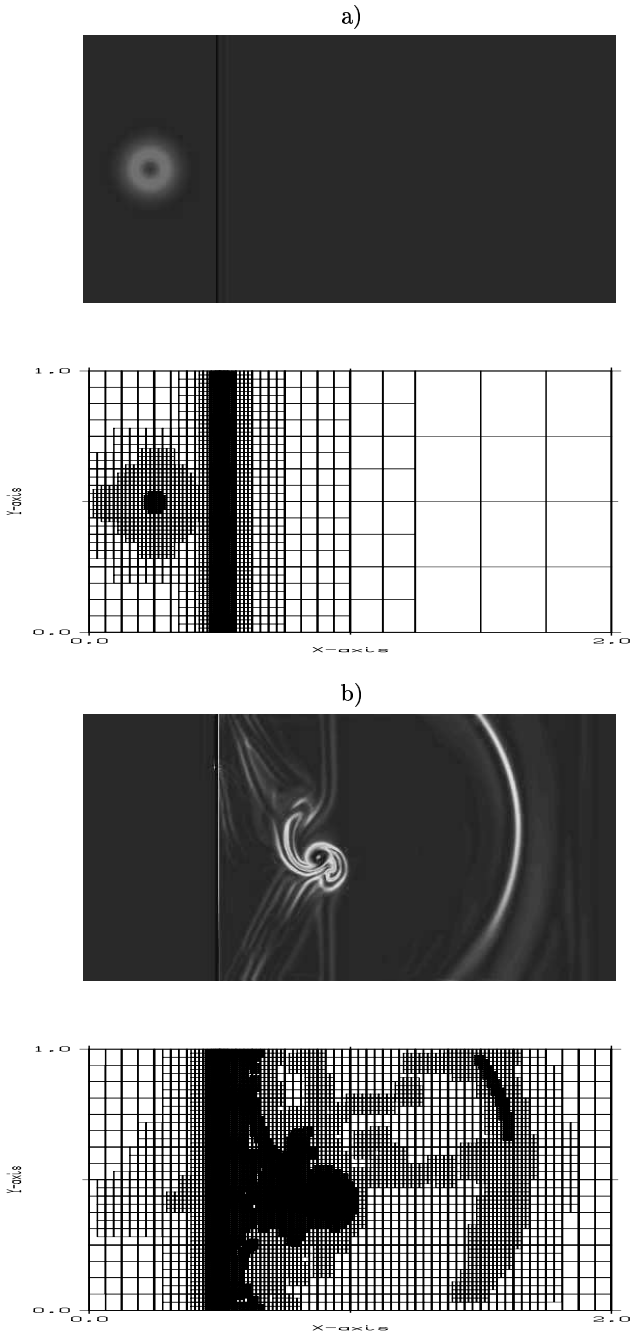

Fig. 8. *Schlieren pictures of the density field of a Mach 4 shock-vortex interaction and associated multilevel grids. a) time* $t = 0$*, b) time* $t = 0.4$.

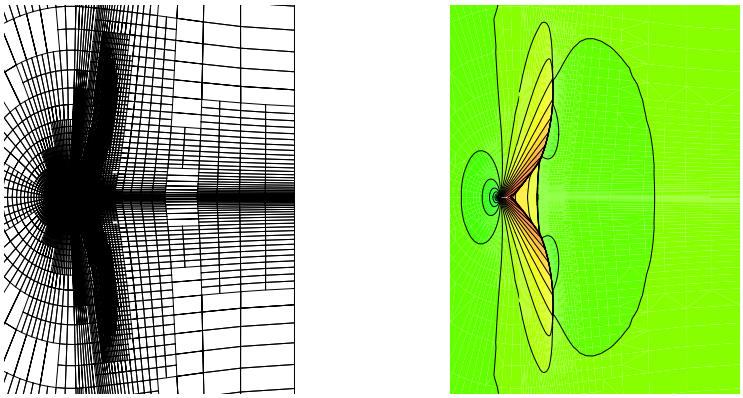

Fig. 9. Total view of NACA0012 airfoil, $M = 0.95$, $\alpha = 0.0^{\circ}$. *Left Figure*: Computational grid. *Right Figure*: Pressure distribution, $M_{min} = 0.0$, $M_{max} = 1.45$, $\Delta M = 0.05$

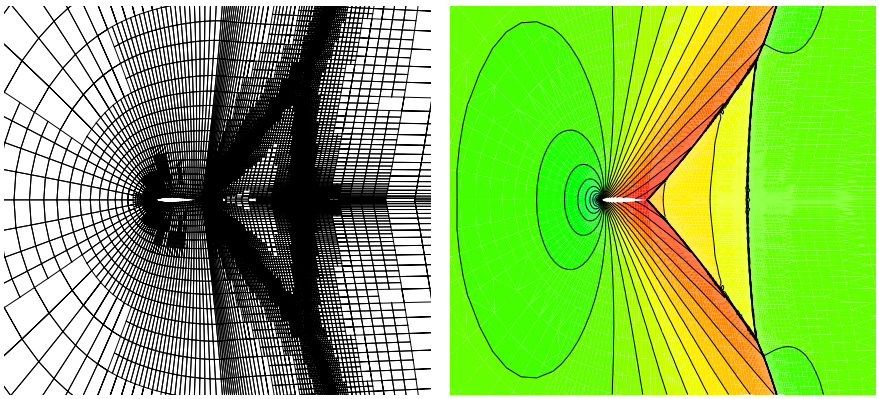

Fig. 10. Detail of Fig. 9